# Monte Carlo analysis of electron transport in GaInAsSb material

A. A. EL OUCHDI[1,*], Y. BELHADJI[2], I. CHIALI[3], N. TAHIR[1], I. ABDELLAOUI[4]
*[1]Division Microélectronique et Nanotechnologies, Centre de Développement des Technologies Avancées, Algiers, Algeria*
*[2]Electrical and Engineering Department, Faculty of Applied Sciences, University of Tiaret, Tiaret, Algeria*
*[3] Electrical Engineering and Industrial Computing Department, National School of Advanced Technology, Algiers, Algeria*
*[4]Division Milieux Ionisés et Laser, Centre de Développement des Technologies Avancées, Algiers, Algeria*

This work presents the results of the ensemble Monte Carlo simulation of electron transport in GaInAsSb material with a stoichiometric coefficient of 0.5. The study focuses on the electrons' behaviour across the three lowest valleys of the conduction band Γ, L, and X considered isotropic and non-parabolic. The main goal is to track the electron trajectories under varying electric fields and temperatures. The dominant scattering mechanisms considered include acoustic and polar optical phonon, as well as inter-valley and intra-valley interactions. The results indicate that both temperature and electric field significantly influence the electronic drift velocity in stationary and transient regimes.

## 1. Introduction

In recent years, the tremendous need for new electronic devices operating in the most advanced applications has led the research toward using new alloy materials [1]. Indeed, nearly all electronic and optoelectronic devices have been realized using alloys of III-V materials [2]. III-V antimonide-based materials are one of these materials. They comprise at least Sb material and other III-V elements [3]. These materials have gained the high attention of researchers and are regarded as good materials operating in such circumstances for their large number of applications, especially in high-frequency operations with much lower power consumption. The quaternary $Ga_xIn_{1-x}As_ySb_{1-y}$ material with stoichiometric coefficients *x* and *y* is one of the antimonide-based materials having interesting properties (low direct band gap, high mobility, low effective masses, robust, etc.). It has mixed properties of the binary materials that constitute it, i.e. GaAs, InAs, GaSb, and InSb [4]. All parameters of this material can be adjusted following Vegard's laws by controlling stoichiometric coefficients [5]. This material has also the capability to be fabricated lattice matched to GaSb [band gap from 0.30 to 0.71 eV], InAs [band gap from 0.36 to 0.69 eV], or InP [band gap from 0.71 to 0.86 eV] substrate by the mean of the liquid phase epitaxy (LPE), the metal-organic chemical vapor deposition (MOCVD) and the molecular-beam epitaxy (MBE) techniques [6] . The research involving this material goes back to the eighties of the last century, where the basic properties were studied. Over time, the research has increased to include the fabrication of complex devices based on this material [7] [8] [9] [10]. The GaInAsSb semiconductor alloys have a wide range of applications. Indeed, it is one of the leading materials used for renewable energy, especially in the photovoltaic field where it is used for the fabrication of high-efficiency multi-junction solar cells [11]. In addition, this material is also used in thermos-photovoltaic systems (TVP) that utilize the thermal radiations of highly heated sources to directly generate electric power [12] [13] [14] [15]. These systems are widely used in the industrial field and serve as a waste heat recovery technique. They can be obtained using four main devices: a generator to provide heat energy from combustion processes, a radiator to translate the thermal energy into an emission spectrum, a filter to coordinate the emission spectrum to a TPV cell, and finally a TPV cell to convert photon radiation into electrical energy [16]. For this, TPV cells based on GaInAsSb lattice matched to GaSb substrate have demonstrated high external quantum efficiencies in the mid-infrared spectral range, making them promising candidates for waste heat recovery from high-temperature "blackbody" sources [17]. As other antimonide-based materials, this material is also an important material for microelectronics and the related field of research since it is regarded as a good candidate for fabrication of the third generation of high electron mobility transistors (HEMT) and heterojunction bipolar transistors (HBT) [18] [19] [20]. Moreover, since the bandgap of antimonide materials can be adapted to cover the entire spectral range of infrared detection by adjusting only the composition coefficient, antimonide-based materials are the most suitable for the design of third-generation Infrared detectors [21] [22]. Furthermore, in infrared lasers, antimonide-based compound semiconductors are important materials of mid-infrared lasers the fact that researchers have made a series of important research such as AlGaAsSb/InGaAsSb multi-quantum well lasers and middle and far-infrared quantum cascade lasers [21] [23]

[24] [25]. Despite the variety of applications of GaInAsSb material, the lack of work and comprehensive data on its intrinsic properties and material parameters remains a significant obstacle, especially with the stoichiometric coefficient of 0.5. To advance the use of this material in practical applications, more detailed studies are essential. The knowledge of the behavior of electrons in the conduction band in the stationary and transient regimes under the application of external forces such as electric field and temperature in this material is one of the interesting areas of research. Indeed, the electrons movement is described using the Boltzmann equation. As this equation is difficult to solve analytically, the use of numerical methods to solve it such as the Monte Carlo method is necessary. In the following section, we provide an overview of the Monte Carlo method applied to electronic transport. In the last section, we present the results of different interaction rates as a function of energy as well as the influence of temperature and electric field on the drift velocity in the stationary and transient regimes.

## 2. Monte Carlo method

To determine the movement of electrons in response to external forces, it is necessary to resolve the Boltzmann equation and determine the distribution function of electrons. The Boltzmann equation is given by the following equation [26] [27]:

$$\frac{\partial f}{\partial t} + v.\nabla_r f + \frac{1}{\hbar} F.\nabla_k f = \left(\frac{\partial f}{\partial t}\right)_{coll} \qquad (1)$$

where $f(r,k,t)$ is the distribution function of electrons in the conduction band, it represents the probability of finding at a time $t$, a carrier at the position $r$, and the wave vector $k$. Since the solution of the Boltzmann equation is almost impossible to reproduce analytically, so, several methods are used to solve it. Among the powerful methods for predicting the non-equilibrium carrier transport in semiconductor materials and devices and giving precise solutions is the simulation based on the Monte Carlo method. The advantage of the Monte Carlo method is its capability to describe complex band structures and provide accurate quantum mechanical treatments of scattering mechanisms. For this, the trajectory of electrons during their movements is followed in real space and the space of wave vectors over time. The band structure taken into consideration is described using the dispersion relation:

$$\varepsilon(1+\alpha\varepsilon) = \frac{h^2 k^2}{2m^*} \qquad (2)$$

where $\varepsilon$ is the electron energy, $\hbar$ represents Planck constant, $k$ is the electron wave factor, $m^*$ is the electron effective mass and $\alpha$ is the non-parabolic coefficient given by:

$$\alpha = \frac{1}{E_g}\left(1-\frac{m^*}{m^e}\right)^2 \qquad (3)$$

with $E_g$ and $m^e$ are the energy gap and the free electron mass respectively.

The dynamic of electrons is assumed divided into free flights followed by scattering mechanisms, which change the energy and the momentum of electrons. The trajectory of electrons during their movements in the real space and the space of the wave vectors is then followed over time. In the absence of external forces, it is given by the following equations:

$$\begin{cases} \dfrac{dk}{dt} = -\dfrac{1}{\hbar} eE \\ \dfrac{dr}{dt} = \dfrac{\hbar}{m^*} k \end{cases} \qquad (4)$$

where $E$ represents the electric field, $e$ is the electron charge $r$ and $k$ represent the position and the wave vector respectively.

The duration of the free flight is calculated using the self-scattering approach. This approach aims to introduce an additional fictive interaction that does not affect the trajectory of electrons and makes the total interaction probability constant $\Gamma$. The free flight duration is calculated using a random number $r$ which varies between $0$ and $1$ as expressed in the following equation:

$$\Delta t = -\frac{1}{\Gamma}\ln(r) \qquad (5)$$

when an external force is applied, electrons change from their initial state ($k(t), r(t)$) at time $t$ to the final state ($k(t+\delta t), r(t+\delta t)$) at time $t_f$, during a brief time $\delta t$. Therefore, the electrons evolve, in the absence of any interaction following these two equations:

$$\begin{cases} k(t+\delta t) = k(t) - \dfrac{eE}{\hbar}\delta t \\ r(t+\delta t) = r(t) + \dfrac{\hbar}{m^*} k(t)\delta t \end{cases} \qquad (6)$$

The scattering mechanisms are selected stochastically based on probabilities related to the microscopic description. If the interaction occurs, the new position and the wave vector are redefined. Otherwise, the state of the electron remains unchanged, however, the free flight process is repeated and another scattering will be selected. This process repeats defining the complex dynamics of electrons in semiconductor materials.

## 3. Simulation results

Applying the Monte Carlo method to GaInAsSb material enables a detailed exploration of its electronic transport characteristics, which is essential due to the limited experimental data available for this material. The simulation provides insights into the various scattering mechanisms, electron drift velocity, temperature and electric field effects [28]. The simulation aims to follow the trajectory of 20,000 electrons under different electric fields (from 1 to 20 kV/cm) and different temperatures (from 100 to 500 K). The simulator takes into account the description of the three lowest valleys of the conduction band $\Gamma$, L, and X isotropic and non-parabolic and centred on the first Brillouin zone [29]. The description of the band structure is the important step of the simulation in which all necessary parameters are described (energy gap, effective masses, energy separation between the different valleys …) [30]. In addition, the scattering mechanisms included in the simulations are those with acoustic and polar optical phonons, as well as intra-valley and inter-valley interactions [28]. The simulator begins first by reading the material parameters. After that, input data are provided, including the number of particles simulated (Ns), the time step, the applied electric field, and the maximum simulation time (Ts). During execution, the simulator performs two key tasks and generates two types of output files. The first file type records the values of various interactions, whereas the second type contains the average quantities, such as drift velocity and valley occupations.

### 3.1. Electronic interactions

#### 3.1.1. Acoustic interactions

The evolution of acoustic interactions for each valley as a function of the energy is depicted in Fig. 1. These interactions are neglected in the $\Gamma$ valley while they become important for the L and in particular in the X valleys. Since these interactions are elastic, the energy of electrons remains unchanged.
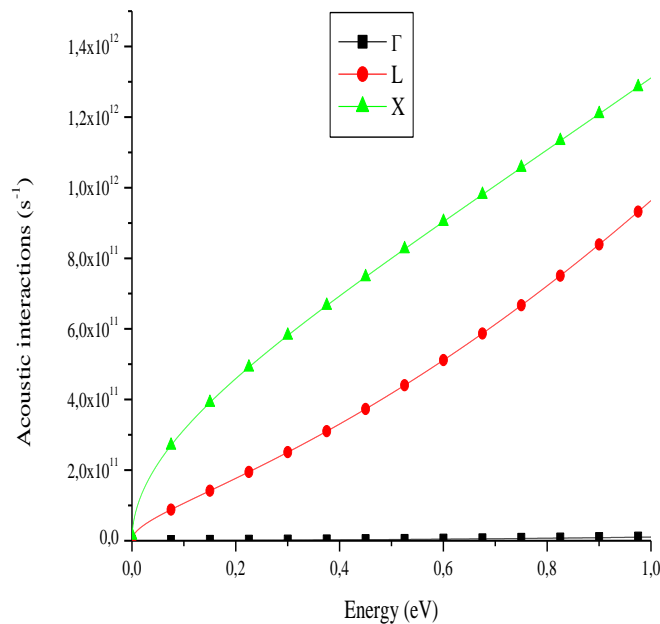


Fig. 1. Acoustic interactions for each valley as a function of energy (color online)

#### 3.1.2. Polar interactions

The evolution of polar optical interactions as a function of energy for each valley in both emission and absorption cases is illustrated in Fig.2. These inelastic interactions change the energy of electrons through the absorption or emission of optical phonons. Phonon emission occurs only when electron energy exceeds the polar optical phonon by approximately 30 meV, corresponding to the theoretical value of the material, making emission interactions more dominant than absorption. In contrast, absorption can occur even at low energies since the phonon energy can always be absorbed. Consequently, emission interactions are more significant than absorption interactions.
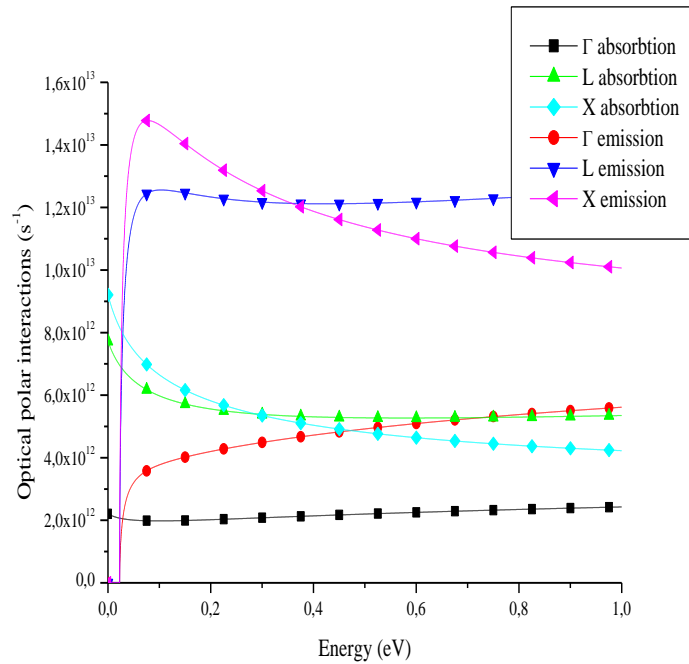
*Fig. 2. Polar optical interactions as a function of energy for each valley in both emission and absorption cases (color online)*

### *3.1.3. Inter-valley interactions*

The evolution of inter-valley interactions for emission and absorption is presented in Fig.3 and Fig.4 respectively. Transitions to higher valleys occur through phonon absorption, where the required phonon energy is determined by the energy difference between the different valleys: about 0.56 eV for $\Delta E_{\Gamma\text{-}L}$, 0.90 eV for $\Delta E_{\Gamma\text{-}X}$, and 0.34 eV for $\Delta E_{L\text{-}X}$, corresponding to the theoretical value of the material. However, transitions to lower valleys can occur even at low electron energies since they do not require additional energy. We note also that emission interactions are generally more important than absorption.
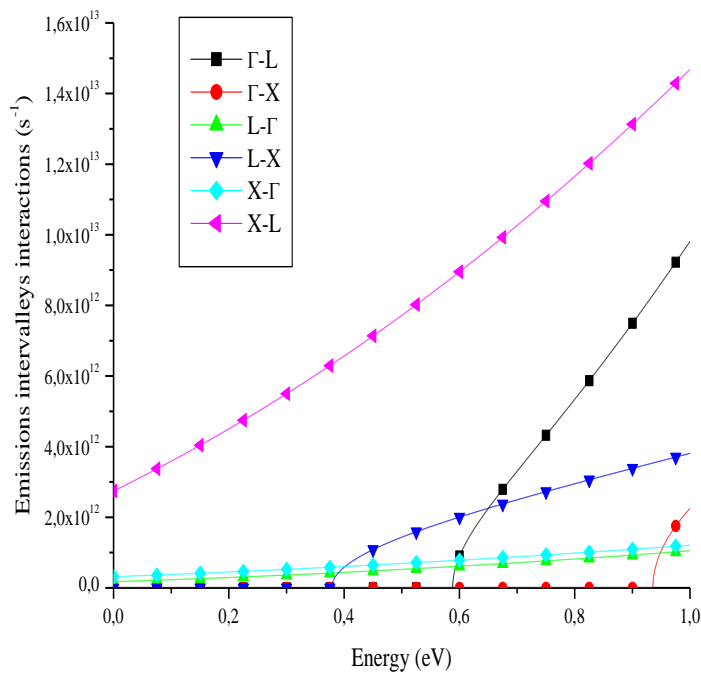


*Fig. 3. Emission inter-valley interactions as a function of energy (color online)*
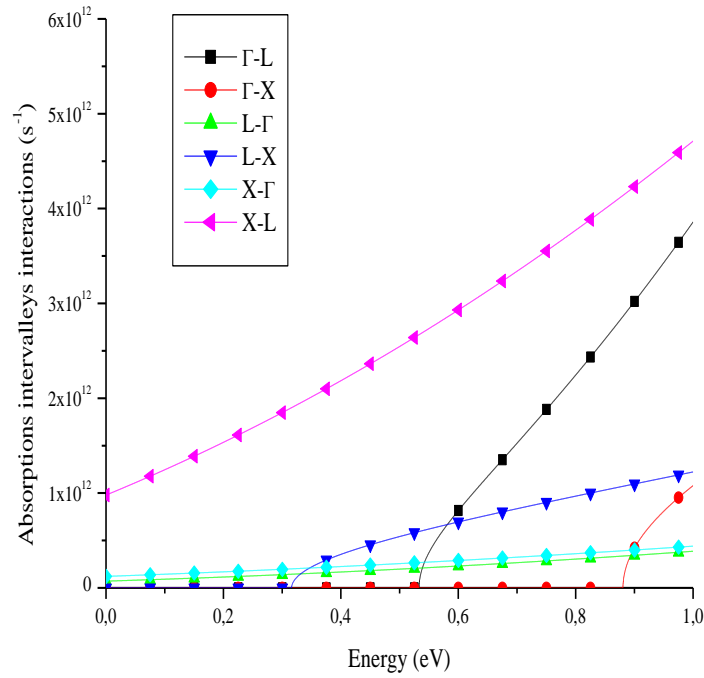
*Fig. 4. Absorption inter-valley interactions as a function of energy (color online)*

### 3.1.4. Valleys occupation

The evolution of valley occupation as a function of the electric field is represented in Fig. 5. At a low electric field, electrons predominantly occupy the central valley. As the energy of electrons increases and reaches the value corresponding to $\Delta E_{\Gamma\text{-}L}$, the transfer of electrons to the L valley accelerates, leading to an inversion in the population. The transfer to the X valley remains low because not only $\Delta E_{\Gamma\text{-}X}$ is relatively large, but also the transfer from L to X valley is low because electrons arriving in L valley do not have sufficient energy to reach X valley.
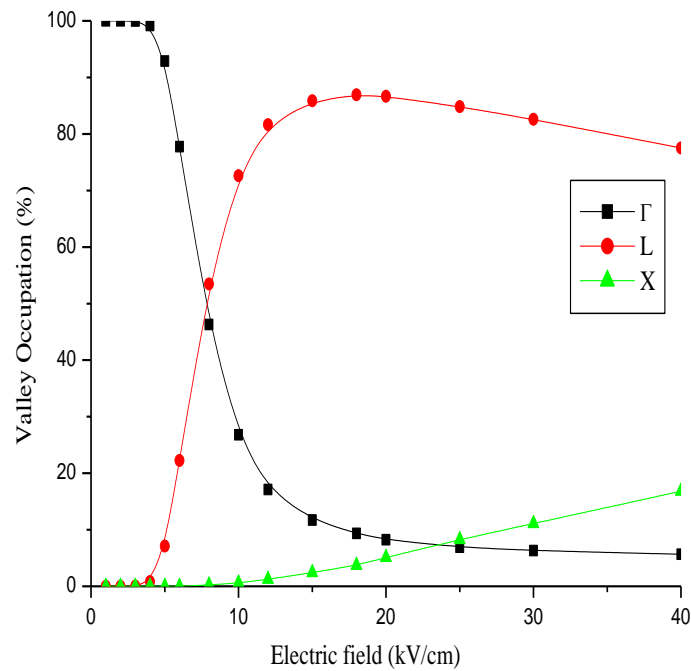


*Fig. 5. Valley occupation as a function of the electric field (color online)*

### 3.2. Electronic drift velocity

#### 3.2.1. Effect of the temperature and electric field on the drift velocity in the transient regime

The evolution of electronic drift velocity as a function of time at E= 10kV/cm for different temperatures is illustrated in Fig.6. Initially, the velocity rapidly increases, reaching an overspeed of approximately $V=6\times10^7$ cm/s at T=300 K. After that, the velocity decreases and stabilizes about $V=1.85\times10^7$ cm/s when the stationary regime is reached. The value of the overspeed is more important than the stationary regime. The overspeed occurs because, at the onset, only a few interactions take place while electrons are rapidly accelerated by the electric field.

When the temperature increases at a constant electric field, the peak velocity decreases due to the increase of the total scatterings.

#### 3.2.2. Effect of the temperature and electric field on the drift velocity in the transient regime

The evolution of electronic drift velocity as a function of time at T=300 K for different electric fields is illustrated in Fig.7. The increase of the electric field at a fixed temperature leads to earlier and more important overspeed values, consequently, it leads to reaching an early stationary regime.
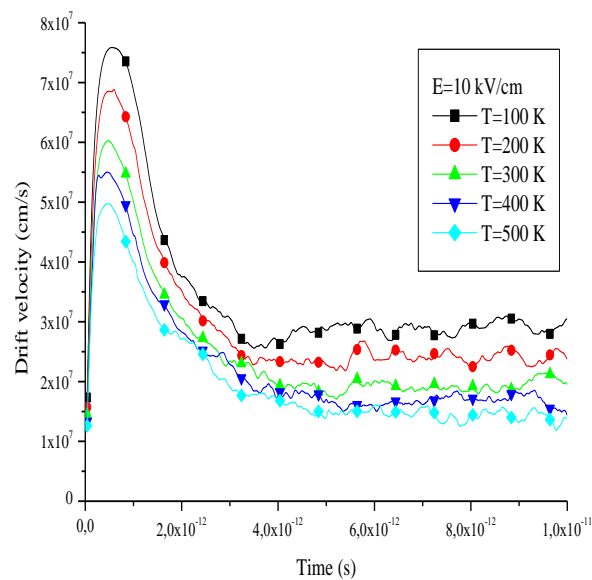


*Fig. 6. Drift velocity as a function of time at E= 10kV/cm for different temperatures (color online)*
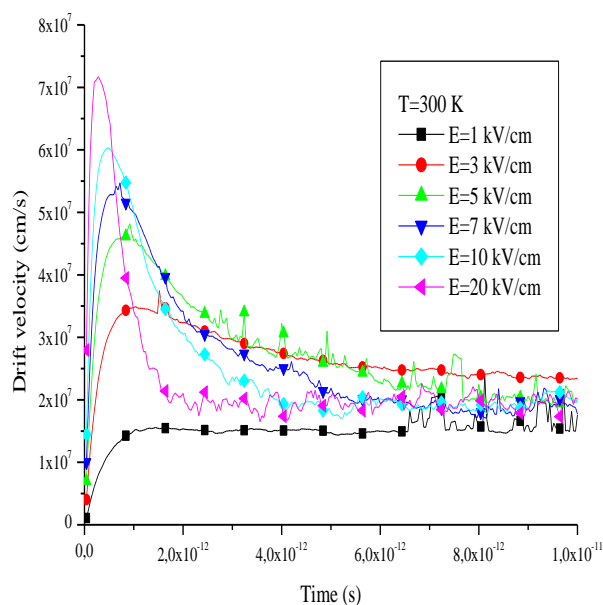


*Fig. 7. Drift velocity as a function of time at T= 300 K for different temperatures (color online)*

### 3.2.3. Effect of the temperature on the drift velocity in the stationary regime

The evolution of electronic drift velocity as a function of the electric field at different temperatures is shown in Fig.8. At low electric fields, the velocity increases linearly with the field, where acoustic interactions dominate. In this case, electrons remain in the $\Gamma$ valley, which has high mobility and low effective mass. As the field increases, the drift velocity rises gradually, reaching a peak of $V=3.6\times10^7$ cm/s at $T=300$ K. At this point, electrons remain in the $\Gamma$ valley, and mainly interact with polar phonons. The electric field at this peak, known as the critical field, is approximately $E=5$ kV/cm at room temperature. This electric field corresponds to the start of electrons transition from the central valley to the satellite valleys (Fig.5). The critical field is heavily influenced by material properties such as bandgap energy, effective masse, and mobility. When the electric field increases more, electrons are transferred to satellite valleys characterized by low electron mobilities. Consequently, the drift velocity decreases and stabilizes, marking the onset of the stationary regime. Here, the velocity remains constant at around $V=1.85\times10^7$ cm/s for $T=300$ K. As in the transient regime, the augmentation of the temperature causes a decrease in the peak velocity. This diminution is due to the augmentation of the overall scattering with temperatures.
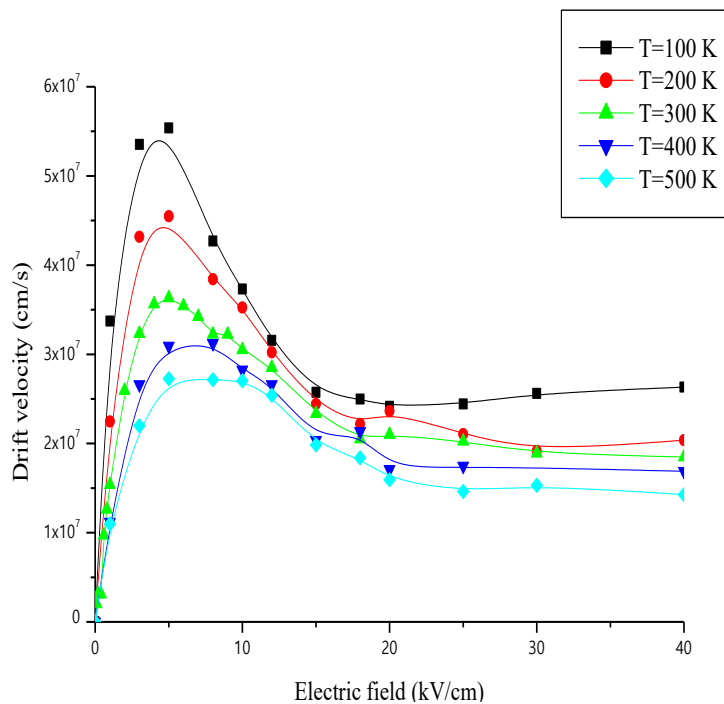


*Fig. 8. Drift velocity as a function of electric field at different temperatures (color online)*

## 4. Conclusion

In this work, the electronic transport properties in GaInAsSb material with a stoichiometric coefficient of 0.5 have been simulated using the ensemble Monte Carlo simulation. The obtained results such as the velocity characteristics are mainly attached to the band structure model and physical parameters especially the effective masses and the energy gap separation between the different valleys. For low values of electric fields, acoustic and polar interactions are dominant. In this case, the velocity increases linearly and reaches the maximum value of $V=3.6\times10^7$ cm/s at about $E=5$ kV/cm for $T=300$ K.

However, at higher values of electric fields, inter-valley interactions are dominated. In this case, the velocity reaches the stationary value $V=1.85\times10^7$ cm/s. The augmentation of the temperature causes a decrease in the peak velocity due to the augmentation of the total scatterings with the temperature in both the transient and the stationary regimes. The augmentation of the electric field causes an increase in the peak velocity of electrons in the transient regime.

## References

[1] S. Adachi, Properties of Semiconductor Alloys: Group-IV, III-V and II-VI Semiconductors, John Wiley & Sons, Ltd., 1 (2009).

[2] H. Arabshahi, M. R. Khalvati, M. R. Rokn-Abadi, Modern Physics Letters B **22**(18), 1777 (2008).

[3] C. Liu, Y. Li, Y. Zeng, Engineering **02**(08), 617 (2010).

[4] B. Wu, G. Xia, Z. Cheng, B. Liang, Z. Li, 6th International Conference on Solid-State and Integrated Circuit Technology. Proceedings (Cat. No.01EX443) **2**, 1289 (2001).

[5] M. Levinshtein, S. Rumyansev, M. Shur, Handbook Series on Semiconductor Parameters: Ternary and Quaternary III–V Compounds, vol. **2**, World Scientific, Singapore, 1996.

[6] J. G. Cederberg, M. J. Hafich, R. M. Biefeld, M. Palmisiano, Journal of Crystal Growth **48**, 289 (2003).

[7] S. Adachi, Journal of Applied Physics **61**(10), 4869 (1987).

[8] S. Ilahi, A. Khalfaoui, F. Genty, N. Yacoubi, Optics and Laser Technology **137**, 106819 (2021).

[9] S. Yip, L. Shen, J. C. Ho, Nanotechnology **30**(20), 202003 (2019).

[10] M. S. Othman, K. A. Mishjil, N. F. Habubi, Chinese Physics Letters **29**(3), 037302 (2012).

[11] S. Parola, A. Vauthelin, F. Martinez, J. Tournet, J. El Husseini, J. Kret, E. Qbesnel, Y. Rouillard, E. Tournié, Y. Cuminal, 7th World Conf. Photovolt. Energy Conversion, WCPEC 2018 - A Jt. Conf. 45th IEEE PVSC, 28th PVSEC 34th EU PVSEC, IEEE Xplore, 937 (2018).

[12] M. G. Mauk, V. M. Andreev, Semiconductor Science and Technology **18**(5), S191 (2003).

[13] A. Karalis, J. D. Joannopoulos, Scientific Reports **7**(1), 1 (2017).

[14] W. E. S. W. A. Rashid, P. J. Ker, M. Z. Bin Jamaludin, M. M. A. Gamel, H. J. Lee, N. B. A. Rahman, IEEE Access **8**, 105156 (2020).

[15] S. Chen, Y. Guo, Q. Pan, Y. Shuai, International Journal of Extreme Manufacturing **6**(2), 022009 (2024).

[16] M. M. A. Gamel, H. J. Lee, W. E. S. W. A. Rashid, P. J. Ker, L. K. Yau, M. A. Hannan, Md. Z. Jamaludin, Materials **14**(17), 4944 (2021).

[17] Q. Lu, R. Beanland, D. Montesdeoca, P. J. Carrington, A. Marshall, A. Krier, Solar Energy Materials and Solar Cells **191**, 406 (2019).

[18] S. M. Bedair, T. Katsuyama, P. K. Chiang, N. A. El-Masry, M. Tischler, M. Timmons, Journal of Crystal Growth **68**(1), 477 (1984).

[19] W. Quan, A. M. Arabhavi, R. Flückiger, O. Ostinelli, C. R. Bolognesi, IEEE Electron Device Letters **39**(8), 1141 (2018).

[20] S. Hamzeloui, A. M. Arabhavi, F. Ciabattini, R. Fluckiger, D. Marti, M. Ebrahimi, O. Ostinelli, C. R. Bolognesi, IEEE Journal of Microwaves **2**(4), 660 (2022).

[21] A. A. El Ouchdi, B. Bouazza, Y. Belhadji, N. Massoum, Semiconductors **51**(12), 1588 (2017).

[22] A. M. Arabhavi, R. Chaudhary, R. Fluckiger, D. Marti, S. Hamzeloui, F. Ciabattini, W. Quan, M. Leich, O. Ostinelli, C. R. Bolognesi, Journal of Lightwave Technology **39**(7), 2171 (2021).

[23] F. Hadjaj, A. Belghachi, M. Belhadj, Energy Procedia **18**, 61 (2012).

[24] Y. G. Zhang, Y. L. Zheng, C. Lin, A. Z. Li, S. Liu, Chinese Physics Letters **23**(8), 2262 (2006).

[25] Q. Lu, A. Marshall, A. Krier, Materials **12**(11), 1743 (2019).

[26] R. W. Kelsall, IEE Colloquium on Physical Modelling of Semiconductor Devices, London, UK, 3/1 (1995).

[27] Y. Belhadji, B. Bouazza, A. A. El-Ouchdi, 5th International Conference on Electrical Engineering - Boumerdes (ICEE-B), 1 (2017).

[28] D. Vasileska, S. M. Goodnick, Computational Electronics: Semiclassical and quantum device modeling and simulation, CRC Press **1**(1), 782 p. (2006).

[29] P. Lugli, Microelectronic Engineering **19**(1-4), 275 (1992).

[30] A. Mostefai, Journal Nano-and Electronic Physics **14**(4), 2 (2022).

_____

*Corresponding author: elouchdi.amine@gmail.com